OPTICA

Er-doped silica fiber laser made by powder-based additive manufacturing

Pawel Maniewski,[1,2,*] Martin Brunzell,[1] Laura Barrett,[1] Clarissa M. Harvey,[1] Valdas Pasiskevicius,[1] and Fredrik Laurell[1]

[1]Department of Applied Physics, KTH Royal Institute of Technology, Stockholm, Sweden
[2]Optoelectronic Research Centre, University of Southampton, Southampton, UK
*pawelma@kth.se

Received 19 April 2023; revised 24 August 2023; accepted 28 August 2023; published 27 September 2023

The pursuit of advanced fiber laser technologies has driven research toward unconventional manufacturing techniques. In this work, we present an erbium-doped fiber laser made using powder-based additive manufacturing. An Er^{3+}/Al^{3+} co-doped silica glass rod was printed using laser powder deposition and then used as the core material in a fiber preform. The fiber drawn from the preform exhibited the complete, desired functionality linked to Er^{3+} doping. To demonstrate this, a standing wave laser cavity was formed with the feedback attained from the cleaved ends of the manufactured fiber. The high quality of the fiber is showcased through a low background loss, single-mode operation, a 9.4% laser slope efficiency, and an output of 4.5 mW, limited by the available pump power. This proof-of-concept opens up promising areas for rapid fabrication and development of high-performance fibers and fiber lasers.

https://doi.org/10.1364/OPTICA.493601

1. INTRODUCTION

Silica glass is widely used as a decorative and technological material in, for example, packaging, tableware, window sheets, optics, and optical cables. Glass is commonly made by rapid cooling (so-called quenching) of its molten form [1]. This fabrication approach is suitable for various consumer products, but other more advanced techniques are preferred to achieve the ultrahigh purity necessary for high-performance devices (e.g., specialty fibers). Although specialty fibers used in lasers or amplifiers can be made using various host materials such as polymers, phosphate, and fluoride glass [2–7], silica glass is highly desirable due to its superior optical properties, robustness, and easy integration with an existing infrastructure [8]. For high-performance silica, advanced manufacturing techniques include, for example, outside vapor deposition (OVD) or modified chemical vapor deposition (MCVD) [9]. Modification of ultrapure silica is typically done by introducing additional dopants to the glass; i.e., to control the refractive index (RI), generate gain, or increase the solubility of other dopants to prevent clustering. These objectives can be achieved concurrently through co-doping with Ge^{4+} and Al^{3+} [10–14]. A specific example of such functional, multicomponent glass compositions are rare-earth (RE) ion co-doped glasses, which are used in fiber lasers and fiber amplifiers [9,13]. When a complex, multicomponent glass composition is required, the conventional fabrication procedure can be time-consuming and expensive. Furthermore, it may lead to variations in the composition at the center of the preform [15,16], which can lower device efficiency.

Additive manufacturing (AM), also referred to as 3D printing, is an attractive fabrication option, where reduced waste and short production cycles are widely recognized. Today, AM is commonly used to make single components as well as working prototypes. Although AM of silica-based glass is challenging, several techniques have been demonstrated in recent years. These can be either a multistep procedure using silica nanocomposites [17–20], a single-step method such as glass filament fusing [21–25], or glass powder sintering [26,27]. Laser powder deposition (LPD) is a technique derived from laser cladding [28,29], where the combination of submicron silica powders and mid-IR CO_2 laser melting allows highly transparent objects to be printed [27]. In recent years, AM of fiber preforms, and thus optical fibers, was demonstrated using polymers [30], low melting temperature glasses [31], the silica nanocomposites mentioned earlier [32,33], and also silica fibers with preforms fabricated using the LPD technique [34]. However, the practical use of AM passive fibers has so far been limited by their high transmission loss [34,35].

In this work, we demonstrate an Er-doped fiber laser (EDFL), based on a high-quality gain fiber made via powder-based AM. First, we used LPD to print an Er^{3+}/Al^{3+} co-doped silica glass rod. The rod was then sleeved into a quartz tube, and collapsed and drawn into a 125 μm diameter fiber. A section of the fiber was then pumped at the Er^{3+} absorption peak ($\lambda_p = 976$ nm) and a strong emission was detected in the telecom C-band, indicating a high-quality fiber. This showed that the fiber can be suitable as the gain fiber in an EDFL. To demonstrate this, a laser cavity was formed using the Fresnel reflections from the air–glass interface at

the cleaved ends of the gain fiber (R ≈ 3.5%). Even with this small feedback, the lasing at the emission peak at 1532 nm ($^4I_{13/2}-^4I_{15/2}$ transition) was observed when the fiber was pumped with a laser diode operating at 976 nm. A maximum power output of 4.5 mW was achieved with a 9.4% slope efficiency. This highlights that our unconventional AM approach using LPD can produce high-quality gain fibers for fiber lasers. Although demonstrated here for Er^{3+}-doped gain fiber fabrication, this AM approach can be readily extended to other rare-earth oxides. Crucially, the method gives flexibility in terms of fast optimization of the fiber core compositions, potentially reducing the time and cost of new fiber development.

2. SILICA FIBERS VIA LASER POWDER DEPOSITION

The rapid prototyping procedure for silica fibers was used to make the gain fiber used in this work, as shown in Fig. 1 and [34]. To achieve the glass composition necessary for the active fiber, a mixture of three submicron powders was prepared: fumed SiO_2 (as a glass-forming host), alumina (Al_2O_3) (for RI control [10]), and erbium oxide (Er_2O_3) (for gain properties). Table 1 shows the raw materials and their ratio in the final powder blend. To achieve the desired properties of the fiber, the powder composition was designed using the doping parameters investigated in [34]. Here, an NA of approximately 0.1 was expected when using 5.7 wt. % of alumina [34]. The Er_2O_3 concentration of 0.7 wt. % was used to directly evaluate LPD impact on the gain performance when compared to other works [36,37]. A total of 150 g of the powder mixture was processed using a ball mill until a homogeneous powder distribution was achieved. The mixture was fed into the printing chamber via a laser-powder print head. This print head consisted of three powder-feeding nozzles, which were placed symmetrically (120° offset) around a centrally positioned CO_2 laser beam ($\lambda = 10.6\,\mu m$, spot size of 1.1 mm, $P = 47\,W$, $M^2 < 1.3$). A detailed print-head description can be found in [27]. The CO_2 laser beam was used to form a melt pool in a quartz glass substrate (flat plate, 1 mm thick, Plan Optik AG), and subsequently to melt the powder injected into the melt pool. A powder feeding rate of 0.5 g/min was used. A solid glass cylinder with an outer diameter (OD) of 1.2 mm was printed upon vertical translation (1 mm/s) of the print head while feeding the powder, as shown in Visualization 1. Typically, the volume of the printed rod is fully densified, with a partly sintered surface, with a thickness up to 15 μm, similar to the rods shown in [27].

To obtain the core-cladding layout of the preform, the rod was then sleeved in a quartz tube (Goodfellow) and tapered to an OD of 6 mm with a core diameter of 200 μm. This preform was then drawn into a 125 μm OD fiber, with the expected core diameter of ≈ 4.2 μm. The fiber was coated with a UV-curable, high RI, silicone coating (OF-154L, ShinEtsu). A schematic of rapid prototyping of silica fibers is depicted in Fig. 1, and details can be found in [34].

3. METHODS FOR MATERIAL AND FIBER EVALUATION

To initially evaluate the quality and the physical properties of the manufactured glass, we used energy dispersive spectroscopy (EDS) to assess the printed glass composition (AZtec, Oxford Instruments). Measurements were performed on both the printed test rod and the manufactured fiber. Carbon and chromium coatings were used to improve the conductivity of the rod and the fiber, respectively. Additionally, the UV-VIS transmission of a 2 mm long section of the rod, with polished end-faces, was measured using a spectrophotometer (Cary 50, Varian).

To evaluate the transmission properties of the fiber, a fiber-coupled white light source (WhiteLase SC480, Fianium) was butt-coupled to the fiber, while the output was monitored with an optical spectrum analyzer (OSA). The fiber's NA was estimated via measurement of the output divergence angle.

Additionally, the cutback method was used to obtain the transmission loss (α) of the fiber. For the transmission loss α, at the pump wavelength $\lambda_p = 976\,nm$, we used a fiber-coupled laser diode (BL976-SAG300, Thorlabs), butt-coupled to our fiber, and the output was monitored with a power meter (S120C, Thorlabs). For the transmission loss at the wavelengths around the expected amplified spontaneous emission (ASE) (i.e., α at $\lambda_s \approx 1530\,nm$), the counter-propagating ASE signal generated from a commercial Er-doped fiber (M12-980-125, Thorlabs) was used. This signal was then butt-coupled into our fiber. The transmitted signal was monitored with a power meter (S122C, Thorlabs). The

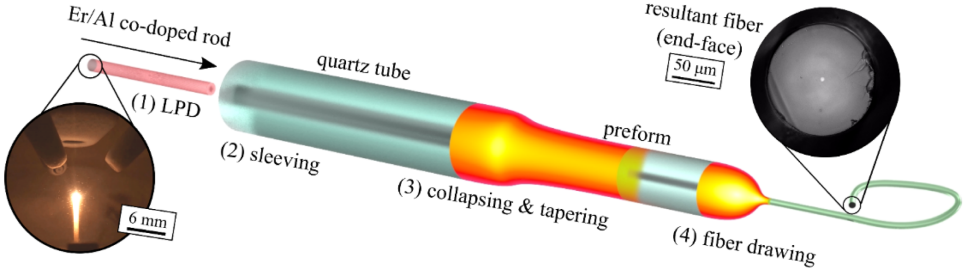

Fig. 1. Sketch of the rapid fiber manufacturing stages: (1) rod making via LPD (see also Visualization 1), (2–3) preform assembly, and (4) fiber drawing. The insets show: (left) a photograph of an ongoing LPD and (right) a micrograph of a typical fiber end face.

Table 1. Powders Used in the Experiments

Powder	Silica (SiO_2)	Alumina (Al_2O_3)	Erbium Oxide (Er_2O_3)	Powder Mixture
Particle size [nm]	≈ 15	≤13	≤100	$SiO_2/Al_2O_3/Er_2O_3$
Manufacturer	Alfa Aesar	Sigma Aldrich	US Research Nanomaterials Inc.	93.6/5.7/0.7 (wt. %)
CAS no.	7631-86-9	1344-08-1	12061-16-4	

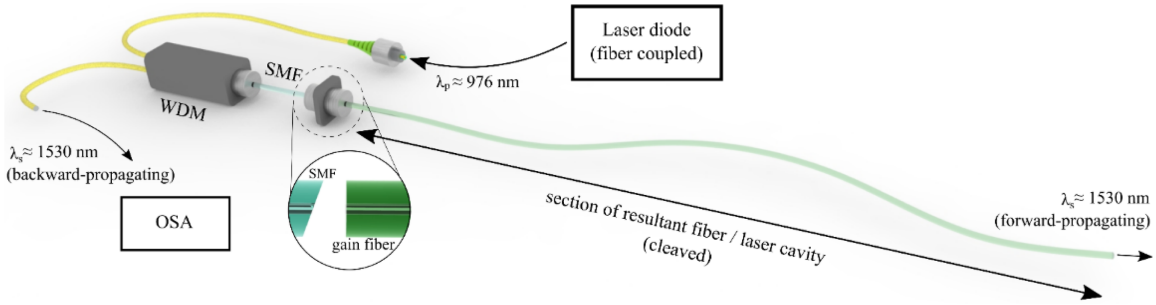

Fig. 2. Schematic of the EDFL arrangement. The bare fiber ends worked as laser mirrors.

cladding modes in these experiments were suppressed by using a RI-matching oil.

A 35 cm long section of the fiber was evaluated as a laser by pumping it with the fiber-coupled 976 nm diode laser (BL976-SAG300, Thorlabs). A fiber-based wavelength division multiplexer (WDM) with an angle polished connector (APC) was used to launch the pump and extract lasing radiation in the backward direction. On both ends of the gain fiber, the cleaved fiber ends acted as cavity reflectors [13,36]; thus, the laser was emitting in both directions, as shown in Fig. 2. The absorbed pump power within the laser was calculated using the α at $\lambda_p = 976$ nm, and residual pump power measured in the forward-propagating end of the laser cavity. Furthermore, the coupling efficiency of 49% between the pump and the gain fiber was established through the ratio of the calculated in-coupled power and the output power of the pump. This was then used to estimate the slope efficiency of the laser. The forward-propagating EDFL beam profile at λ_s was recorded using a pyroelectric camera (Pyrocam III, Ophir Optronics Solutions). Here, a long-pass filter was used to block any residual pump light.

4. EXPERIMENTAL RESULTS

A. Material Properties

A 20 mm long test rod was printed and manually removed from the substrate. Subsequently, the rod was diced into several test samples. Three cuts, parallel to the rod's base, were made using a high-speed rotational saw (DISCO Corp.). To expose the inner volume of the rod (vertical cross-section in Fig. 3), the middle piece was polished longitudinally. A sketch of the prepared samples and obtained spectra are shown in Fig 3. The material composition in different scans corresponded to the powder mixture composition. Additionally, a deviation in average aluminum concentration within each scan, as shown in Fig. 3(c), was $\leq$0.3 wt.% for samples of several printed test rods. During this measurement, the erbium concentration was found below a threshold for a reliable wt% profile estimation. To examine the erbium content, a 2 mm long section of the test rod was used to measure the UV-VIS transmission of the printed rod. Figure 3(c) shows the resulting characteristic Er^{3+} absorption peaks at 380 nm, 520 nm, and 650 nm [13].

One of the fabricated 20 mm long rods was used as a core material in the optical fiber. To achieve a core-cladding layout, the rod was sleeved in a pure quartz tube. The rod-in-tube assembly was collapsed, and then tapered to a final preform, as described in [34]. The preform was then drawn into a fiber using a laser-based fiber drawing tower [38] with a drawing speed of 20 m/min. Figures 4(a)–4(c) show, respectively, the cross-section of the fiber, the obtained EDS spectrum, and the line scan of the composition across the core. The SEM image of the core area, shown in the inset in Fig. 4(a), depicts the visible contrast between the core and cladding, indicating a material difference between them. Using the SEM image, a core diameter of $\approx$4.4 μm was measured.

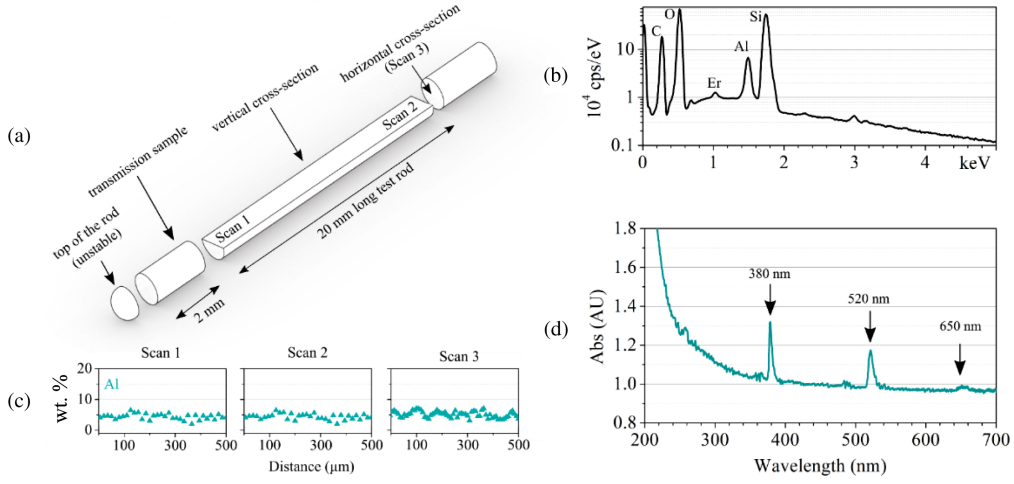

Fig. 3. (a) Schematics of different test samples cut from the printed test rod. (b) Example EDS spectrum from the horizontal cross-section (Scan 3, the carbon peak comes from the carbon coating applied for the EDS measurement) of the test rod. (c) EDS doping profiles for each of the scans shown in (a). (d) UV-VIS absorbance spectrum was measured through the 2 mm long transmission sample.

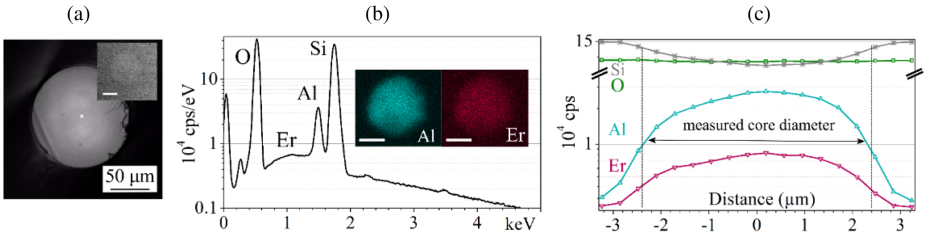

Fig. 4. (a) Micrograph of the manufactured fiber and SEM image (contrast increased) of the core (scale bar corresponds to 2 μm), (b) EDS spectrum retrieved from the core of the fiber. Insets show the dopant distribution in the area around the core (scale bars correspond to 2 μm), and (c) EDS line scan for the core. The displayed, measured core diameter was measured using the SEM image.

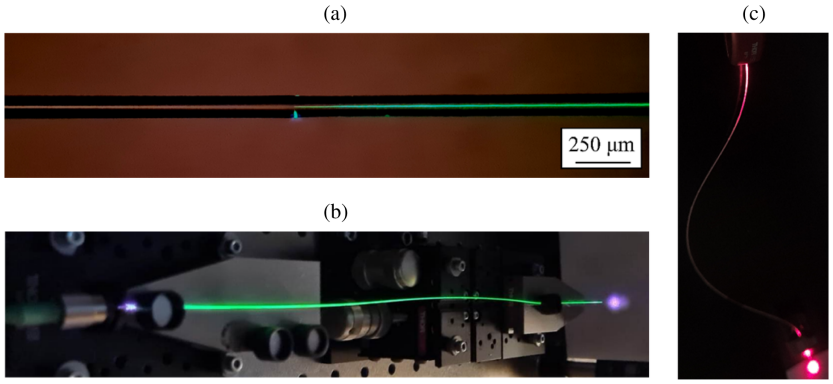

Fig. 5. Micrograph (a) of the manufactured fiber (in right) spliced with commercial passive fiber (in left), and photographs of an approximately 30 cm long section of fiber (b) used as a fiber laser, and (c) guiding fiber-coupled red diode.

B. Fiber Performance

To demonstrate the compatibility of this fiber with other commercial silica fibers, it was spliced with a passive fiber (core diameter of 10 μm, NA = 0.2). Figure 5(a) shows a micrograph of the spliced fibers. Low power (976 nm) was then launched into the passive fiber and green upconversion from the Er ions can be seen in the printed fiber. In Fig. 5(b), the pump was directly butt-coupled via APC to the gain fiber. This layout was later used as the laser cavity, as shown in Fig. 2. The clearly visible green glow in Figs. 5(a) and 5(b) is attributed to the cooperative upconversion from the $^4I_{11/2}$ level and is a nonlinear function of the population of that level. Homogeneous doping is suggested by the uniform glow over the entire length of the fiber under investigation, with no noticeable scattering centers. The latter is further depicted in Fig. 5(c).

The transmission spectrum of the manufactured fiber in Fig. 6 shows the characteristic absorption bands of Er^{3+}, with peaks at λ = 650 nm ($^4F_{9/2}$), 800 nm ($^4I_{9/2}$), 980 nm ($^4F_{11/2}$), and 1530 nm ($^4I_{13/2}$), respectively [39]. To complement this measurement, the transmission loss at the pump ($\lambda_p \approx 980$ nm, $\alpha = 17.3$ dB/m) and at the signal ($\lambda_s \approx 1530$ nm, $\alpha = 23.9$ dB/m) wavelengths were measured by injecting these wavelengths into the fiber at small-signal power levels and using the cutback method. Measurement of the background propagation loss was performed outside the Er-absorption band using a laser operating at 1342 nm. The loss at this wavelength was estimated to be $\alpha \ll 1$ dB/m. The loss was based on seven cutbacks, while the complete representation of such low loss was limited by the relatively short length of the fiber (≈0.5 m). Additionally, we verified that the fiber was transversely single-mode at λ_s, and it had an NA of approximately 0.103, estimated via measurement of the output divergence angle. The fiber parameters are listed in Table 2.

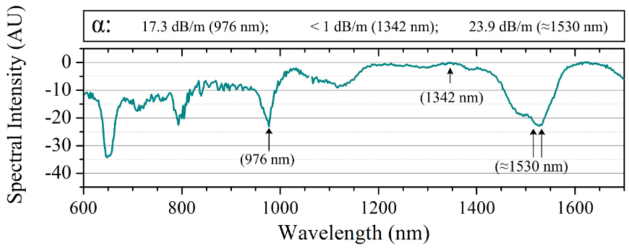

Fig. 6. Transmission spectrum of an approximately 40 cm long fiber measured with the OSA. The loss values (α) marked by arrows in the figure were obtained using cutback measurements.

A 35 cm long section of the fiber was then pumped to characterize the laser properties. It was pumped with the 976 nm diode and the cavity was formed without external mirrors. The feedback was obtained from the end faces of the cleaved fiber. The characteristic laser spectrum is shown in Fig. 7(a) with the emission centered around the Er-gain peak at $\lambda_s = 1532$ nm. The inset shows the beam profile at λ_s measured at a distance of approximately 3 cm from the end face. The fringes visible in the beam profile are a consequence of an uncoated long-pass filter placed in front of the camera used to block any residual pump radiation. The laser threshold was observed at an absorbed pump power of 47 mW with a slope efficiency of 9.4% as shown in Fig. 7(b). The maximum output power of 4.5 mW at $\lambda_s = 1532$ nm was limited by the available pump power. An upper-state lifetime (τ_{LPD}) of 8.4 ms was measured, as shown in Fig. 7(c).

5. DISCUSSION

An Er/Al co-doped silica glass rod was made via LPD and used as the core material in a fiber preform, from which the fiber

Table 2. Parameters of the Manufactured Fiber

OD	Core Diameter	NA	≈ Δn	α (976 nm)	α (1342 nm)	α (≈ 1530 nm)
125 μm	≈ 4.4 μm	≈ 0.103	0.004	17.3 dB/m	<1 dB/m	23.9 dB/m

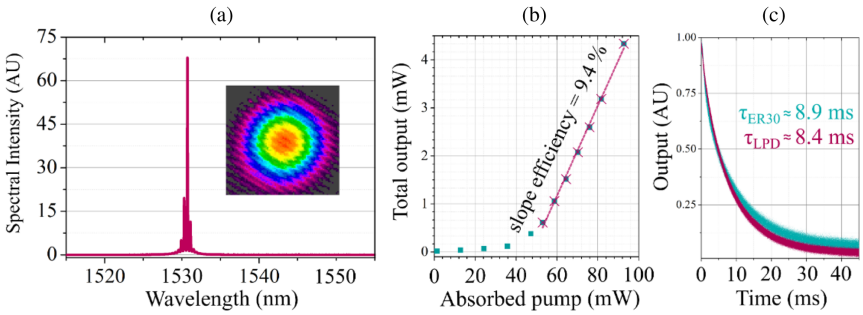

Fig. 7. (a) Output spectrum for the laser. Inset shows the output mode. (b) Output power as a function of absorbed pump power. (c) Comparison of upper-state lifetime curves between our fiber (τ_{LPD}) and a commercial (τ_{ER30}) Er-doped fiber (ER30, Thorlabs).

(OD = 125 μm) was drawn. The small laser-induced hot-zone used in LPD provides higher heating and cooling rates compared to traditional glass-making methods. The heating and cooling dynamics can be observed in the black-body radiation recording in Visualization 1. The rapid, laser-induced heating, combined with different airborne powders, can potentially lead to different deposition and evaporation rates for each of the compounds combined in our powder mixture. However, it was shown that the material composition of the powder mixture was maintained across and along the rod, implying its high homogeneity, as shown in Fig. 3(c). Clearly, the LPD printing process maintained the expected composition. The powder efficiency of our process was measured to be approximately 30% by the ratio between the weight of the printed rod to the weight of the powder used for printing. It is, however, important to mention that due to reduced shadowing effects [29], and thus minimal heating of the airborne powder upon passing the CO_2 laser beam, the unused powder can potentially be collected and reused. We consider it as one of the areas that can be addressed in future work.

In the manufactured fiber, the size of the core measured using the SEM image [Fig. 4(a)] shows that the potential diffusion of dopants reached <0.5 μm into the cladding. Furthermore, EDS analysis of the fiber showed a symmetric doping distribution over the core; note the logarithmic scale in Fig. 4(c). The concentration gradient in Al- and Er- distribution seen in Fig. 4(c) is likely a convolution of the 3 μm diameter EDS probe beam and the actual elemental distribution across the core. The characteristic homogeneous green glow, linked to the upconversion through the pumping level, suggests a homogeneous Er^{3+} doping along the length of the fiber, as shown in Fig. 5(b); note that no visible scattering centers were observed. The high doping levels, with negligible variations in composition in the core, improve gain conditions compared to the typically obtained doping profile [15,16]. Moreover, the clear, characteristic absorption peaks of Er^{3+} and low background loss (Figs. 3 and 6), indicate the high quality of this gain fiber.

The results showcased by this fiber were possible due to several improvements of our earlier work. The periodic undulation of the printed rod's diameter [27] was significantly reduced by improving the mechanical components of the LPD system. This ensured a void-free core-cladding interface of the fiber. Second, based on the experimental data, the composition of the LPD-made glass was altered compared to [34] to increase the step-index profile of the fiber; thus, reducing the bend sensitivity and ensuring stable, single-mode operation. Additionally, we increased the Er_2O_3 to 0.7 wt% in our powder mixture to provide a sufficient concentration of active ions, which is necessary for a relatively short and simple fiber laser.

A 35 cm long section of the fiber was used in a proof-of-concept EDFL. The laser cavity was formed with Fresnel reflections at the air–glass interface at the cleaved ends of the fiber; thus, both ends of the fiber acted as the output couplers with approximate 96.5% output coupling [13]. For cw operation, the gain of the fiber must compensate for the overall loss. The laser operated at the wavelength around 1530 nm, where the gain is highest, but the quasi-three-level nature in this spectral range imposes reabsorption in the unpumped part of the fiber. A population inversion of at least 50% is required to overcome the reabsorption losses and achieve gain. The fact that lasing occurred at 1530 nm suggests that the RE ion clustering is limited because the upconversion rate is a nonlinear function of the upper state concentration. It should also be noted that elements for wavelength stability control, such as fiber Bragg gratings, can be implemented for further laser spectra stabilization. However, such a laser optimization is well-known and outside the immediate scope of this work. To give further context regarding the 9.4% slope efficiency obtained in this work, Kimura *et al*. used a similar laser configuration and core composition [36] and achieved a 6.3% slope efficiency for a 7 m long Er-doped fiber, fabricated using MCVD with solution doping. It was pumped at $\lambda = 1.48$ μm, a wavelength where the EDFL typically gives a 1.5 higher slope efficiency compared to pumping at $\lambda_p = 976$ nm [13], which also highlights the quality of the fiber fabricated using our method.

6. CONCLUSION

In summary, by implementing laser-based additive manufacturing, we fabricated a single-mode Er/Al co-doped gain fiber and evaluated it as a fiber laser at 1530 nm. A solid silica glass rod was printed via LPD (i.e., a dry nano-powder mixture was laser sintered), and then the rod was used as a core in fiber preform, which was drawn into the fiber.

The printed rods, as well as the resultant gain fiber, showed low composition variations e.g., between the different sections of the rod, the aluminum variation was smaller than 0.3 wt. %. Both the printed glass and the resultant fiber showed distinct absorption peaks, while the peaks at 980 nm and 1530 nm are indicative of strong unquenched Er^{3+}-ion doping. Outside of the Er^{3+} absorption bands, namely at 1342 nm, a low loss of $\ll 1$ dB/m was measured.

Lasing was evaluated using a 35 cm long section of the fiber in a simple design, where the cavity was formed by the cleaved ends of the fiber. Even with this small feedback ($R \approx 3.5\%$), lasing was achieved with a low threshold of 47 mW and a high slope efficiency of 9.4%. The relatively long upper-state lifetime of 8.4 ms, further highlights the high quality of the material achieved via LPD.

In short, the gain fiber produced in this study, via AM exhibited complete and intended functionality because of: (i) the single-mode operation, (ii) a low-loss outside of Er^{3+} absorption bands, (iii) high, unclustered doping levels, and (iv) an efficient lasing performance.

This work shows that powder-based glass AM can be a feasible alternative to other, complex methods to make highly doped gain fibers. The achievements highlighted here showcase laser-based manufacturing technologies that could be used for high-performance photonics devices. Although it was demonstrated here for Er^{3+}-doped gain fiber fabrication, this fabrication approach can be readily extended to other rare-earth oxides. Future work will include more complex compositions and work toward rapid material tailoring.

Funding. Vetenskapsrådet (2022-06180); Stiftelsen Tornspiran (877); Stiftelsen för Strategisk Forskning; Knut och Alice Wallenbergs Stiftelse.

Acknowledgment. We acknowledge M. Fokine for topical discussions and the equipment that was used in this project. We thank the Swedish Research Council, Swedish Foundation for Strategic Research, and the K.A. Wallenberg Foundation for the financial support.

Author contributions. P.M. developed the LPD recipe and designed the research; M.B., P.M., V.P., and F.L. designed and characterized the EDFL; C.M.H. made the preform; C.M.H. and P.M. drew the fiber; and L.B. performed and analyzed EDS measurements on the test samples. All authors analyzed and reviewed the results and participated in writing the manuscript. P.M. supervised the project.

Disclosures. The authors declare no conflicts of interest.

Data availability. Data underlying the results presented in this paper are not publicly available at this time but may be obtained from the authors upon reasonable request.

REFERENCES

1. J. E. Shelby, *Introduction to Glass Science and Technology* (Royal Society of Chemistry, 2007).
2. M. Kochanowicz, J. Zmojda, P. Miluski, A. Baranowska, K. Sadowska, M. Kuwik, J. Pisarska, W. A. Pisarski, and D. Dorosz, "Ultra-broadband emission in Er^{3+}/Tm^{3+}/Ho^{3+} triply-doped germanate glass and double-clad optical fiber," Opt. Mater. Express **12**, 2332–2342 (2022).
3. Y. Ohishi, "Supercontinuum generation and IR image transportation using soft glass optical fibers: a review [Invited]," Opt. Mater. Express **12**, 3990–4046 (2022).
4. T.-M. Usher-Ditzian, "SCHOTT laser glass [Invited]," Opt. Mater. Express **12**, 4399–4417 (2022).
5. T. Yamashita, "Nd- and Er-doped phosphate glass for fiber laser," Proc. SPIE **1171**, 291–297 (1990).
6. M. C. Falconi, D. Laneve, V. Portosi, S. Taccheo, and F. Prudenzano, "Design of a multi-wavelength fiber laser based on Tm:Er:Yb:Ho co-doped germanate glass," J. Lightwave Technol. **38**, 2406–2413 (2020).
7. K. Jakubowski, C.-S. Huang, L. F. Boesel, R. Hufenus, and M. Heuberger, "Recent advances in photoluminescent polymer optical fibers," Curr. Opin. Solid State Mater. Sci. **25**, 100912 (2021).
8. L. A. Moore and C. M. Smith, "Fused silica as an optical material [Invited]," Opt. Mater. Express **12**, 3043–3059 (2022).
9. M. Yamane and Y. Asahara, *Glasses for Photonics* (Cambridge University, 2000).
10. J. Wang, "Alumina as a dopant in optical fiber by OVD," Appl. Phys. A **116**, 505–518 (2014).
11. K. A. M. Sharif, N. Y. M. Omar, M. I. Zulkifli, S. Z. M. Yassin, and H. A. Abdul-Rashid, "Fabrication of alumina-doped optical fiber preforms by an MCVD-metal chelate doping method," Appl. Sci. **10**, 7231 (2020).
12. S. Unger, A. Schwuchow, J. Dellith, and J. Kirchhof, "Optical properties of ytterbium/aluminium doped silica glasses," Opt. Mater. Express **10**, 907–925 (2020).
13. M. J. F. Digonnet, *Rare-Earth-Doped Fiber Lasers and Amplifiers*, 2nd revised ed. (Marcel Dekker, 2001).
14. J. L. Wagener, D. J. DiGiovanni, P. F. Wysocki, M. J. F. Digonnet, and H. J. Shaw, "Effects of concentration and clusters in erbium-doped fiber lasers," Opt. Lett. **18**, 2014–2016 (1993).
15. M. Franczyk, D. Pysz, P. Pucko, D. Michalik, M. Biduś, M. Dłubek, and R. Buczyński, "Yb^{3+} doped silica nanostructured core fiber laser," Opt. Express **27**, 35108–35119 (2019).
16. E. Bélanger, J.-P. Bérubé, B. de Dorlodot, P. Marquet, and R. Vallée, "Comparative study of quantitative phase imaging techniques for refractometry of optical waveguides," Opt. Express **26**, 17498–17510 (2018).
17. R. Dylla-Spears, T. D. Yee, K. Sasan, D. T. Nguyen, N. A. Dudukovic, J. M. Ortega, M. A. Johnson, O. D. Herrera, F. J. Ryerson, and L. L. Wong, "3D printed gradient index glass optics," Sci. Adv. **6**, eabc7429 (2020).
18. F. Kotz, K. Arnold, W. Bauer, D. Schild, N. Keller, K. Sachsenheimer, T. M. Nargang, C. Richter, D. Helmer, and B. E. Rapp, "Three-dimensional printing of transparent fused silica glass," Nature **544**, 337–339 (2017).
19. Z. Hong, P. Ye, D. A. Loy, and R. Liang, "Three-dimensional printing of glass micro-optics," Optica **8**, 904–910 (2021).
20. J. T. Toombs, M. Luitz, C. C. Cook, S. Jenne, C. C. Li, B. E. Rapp, F. Kotz-Helmer, and H. K. Taylor, "Volumetric additive manufacturing of silica glass with microscale computed axial lithography," Science **376**, 308–312 (2022).
21. T. Grabe, M. Lammers, S. Wang, X. Wang, K. Rettschlag, K. Sleiman, A. Barroi, T. Biermann, A. Ziebehl, J. Röttger, P.-P. Ley, A. Wolf, P. Jaeschke, J. Hermsdorf, S. Kaierle, H. Ahlers, and R. Lachmayer, "Additive manufacturing of fused silica using coaxial laser glass deposition: experiment, simulation and discussion," Proc. SPIE **11677**, 116770Z (2021).
22. P. von Witzendorff, L. Pohl, O. Suttmann, P. Heinrich, A. Heinrich, J. Zander, H. Bragard, and S. Kaierle, "Additive manufacturing of glass: CO_2-laser glass deposition printing," Proc. CIRP **74**, 272–275 (2018).
23. C. Liu, T. Oriekhov, and M. Fokine, "Investigation of glass bonding and multi-layer deposition during filament-based glass 3D printing," Front. Mater. **9**, 978861 (2022).
24. J. Luo, H. Pan, and E. C. Kinzel, "Additive manufacturing of glass," J. Manuf. Sci. Eng. **136**, 272–275 (2014).
25. D. G. Moore, L. Barbera, K. Masania, and A. R. Studart, "Three-dimensional printing of multicomponent glasses using phase-separating resins," Nat. Mater. **19**, 212–217 (2020).
26. G. Marchelli, D. Storti, M. Ganter, and M. Prabhakar, "An introduction to 3D glass printing," in *Solid Freeform Fabrication Symposium Proceedings* (2021).
27. P. Maniewski, F. Laurell, and M. Fokine, "Quill-free additive manufacturing of fused silica glass," Opt. Mater. Express **12**, 1480–1490 (2022).
28. R. Comesaña, F. Quintero, F. Lusquiños, M. J. Pascual, M. Boutinguiza, A. Durán, and J. Pou, "Laser cladding of bioactive glass coatings," Acta Biomater. **6**, 953–961 (2010).
29. P. Maniewski, F. Laurell, and M. Fokine, "Laser cladding of transparent fused silica glass using sub-μm powder," Opt. Mater. Express **11**, 3056–3070 (2021).
30. D. R. Gozzard, R. Craine, D. Hickey, A. Martin, W. Shen, and B. Sones, "Optical couplers and step-index fibers fabricated using FDM 3D printers," Opt. Lett. **47**, 5124–5127 (2022).
31. J. Carcreff, F. Cheviré, E. Galdo, R. Lebullenger, A. Gautier, J. L. Adam, D. le Coq, L. Brilland, R. Chahal, G. Renversez, and J. Troles, "Mid-infrared hollow core fiber drawn from a 3D printed chalcogenide glass preform," Opt. Mater. Express **11**, 198–209 (2021).

32. Y. Chu, X. Fu, Y. Luo, J. Canning, Y. Tian, K. Cook, J. Zhang, and G.-D. Peng, "Silica optical fiber drawn from 3D printed preforms," Opt. Lett. **44**, 5358–5361 (2019).
33. Y. Chu, X. Fu, Y. Luo, J. Canning, J. Wang, J. Ren, J. Zhang, and G.-D. Peng, "Additive manufacturing fiber preforms for structured silica fibers with bismuth and erbium dopants," Light Adv. Manuf. **3**, 1 (2022).
34. P. Maniewski, C. M. Harvey, K. Mühlberger, T. Oriekhov, M. Brunzell, F. Laurell, and M. Fokine, "Rapid prototyping of silica optical fibers," Opt. Mater. Express **12**, 2426–2435 (2022).
35. Y. Luo, J. Canning, J. Zhang, and G.-D. Peng, "Toward optical fibre fabrication using 3D printing technology," Opt. Fiber Technol. **58**, 102299 (2020).
36. Y. Kimura, K. Suzuki, and M. Nakazawa, "Laser-diode-pumped mirror-free Er^{3+}-doped fiber laser," Opt. Lett. **14**, 999–1001 (1989).
37. W. L. Barnes, P. R. Morkel, L. Reekie, and D. N. Payne, "High-quantum-efficiency Er^{3+} fiber lasers pumped at 980 nm," Opt. Lett. **14**, 1002–1004 (1989).
38. C. M. Harvey, K. Muhlberger, T. Oriekhov, P. Maniewski, and M. Fokine, "Specialty optical fiber fabrication: fiber draw tower based on a CO laser furnace," J. Opt. Soc. Am. B **38**, F122–F129 (2021).
39. H. N. Russell and F. A. Saunders, "New regularities in the spectra of the alkaline earths," Astrophys. J. **61**, 38 (1925).